Observation of a Transition from Fluid to Kinetic Nonlinearities for Langmuir Waves Driven by Stimulated Raman Backscatter

J. L. Kline,[1] D. S. Montgomery,[1] B. Bezzerides,[1] J. A. Cobble,[1] D. F. DuBois,[1] R. P. Johnson,[1] H. A. Rose,[1] L. Yin,[1] and H. X. Vu[2]

[1]*Los Alamos National Laboratory, Los Alamos, New Mexico 87545, USA*
[2]*University of California, San Diego, California 92093, USA*

(Received 5 September 2003; published 4 May 2005)

Thomson scattering is used to measure Langmuir waves (LW) driven by stimulated Raman scattering (SRS) in a diffraction limited laser focal spot. For SRS at wave numbers $k\lambda_D \lesssim 0.29$, where k is the LW number and λ_D is the Debye length, multiple waves are detected and are attributed to the Langmuir decay instability (LDI) driven by the primary LW. At $k\lambda_D \gtrsim 0.29$, a single wave, frequency-broadened spectrum is observed. The transition from the fluid to the kinetic regime is qualitatively consistent with particle-in-cell simulations and crossing of the LDI amplitude threshold above that for LW self-focusing.

DOI: 10.1103/PhysRevLett.94.175003 PACS numbers: 52.38.Bv, 52.35.Fp, 52.35.Mw, 52.38.Dx

Stimulated Raman backscattering (SRS) is a three-wave parametric instability that occurs in laser-irradiated plasmas, whereby an intense laser light wave decays into a scattered light wave and an electron plasma wave, i.e., a Langmuir wave (LW). For target designs relevant to indirect drive inertial confinement fusion [1], the SRS linear gain is large enough such that nonlinear mechanisms are expected to saturate the LW growth [2]. Saturation may occur as the SRS LW dissipates energy into other waves (wave-wave coupling) or into the electrons (wave-particle coupling).

For a LW phase velocity much greater than the electron thermal velocity ($v_\phi/v_e \gg 1$) the effect of electrons trapped in the potential wells of the LW (electron trapping) is relatively weak since there are few particles in this region of the electron velocity distribution $f_0(v)$. In this regime, fluidlike effects, such as Langmuir wave collapse and Langmuir decay instability (LDI) cascade, tend to dominate the nonlinear behavior of LWs [3]. Here, $v_\phi = \omega/k$ is the phase velocity of the LW with frequency and wave number (ω, k), and $v_e = \sqrt{T_e/m_e}$ is the electron thermal velocity, so that these effects occur for small $k\lambda_D$ [$k\lambda_D \approx (v_\phi/v_e)^{-1}$, where the Debye length, λ_D, is the ratio of the electron thermal velocity to the plasma frequency]. For $v_\phi/v_e \sim 1$ (large $k\lambda_D$), the LW interacts with more electrons within the bulk of the electron velocity distribution. In this regime, kinetic effects, such as a reduced Landau damping rate and a nonlinear frequency shift due to electron trapping and eventual loss of resonance [4], are expected to dominate the nonlinear behavior of LWs [5,6].

In this Letter, we report the observation of both fluid (wave-wave) and kinetic (wave-particle) nonlinearities associated with SRS. The experiments are performed using a laser in a single-hot-spot (SHS) configuration [7] to drive SRS in a preformed plasma. Since the SHS dimensions are much smaller than local plasma gradient scale lengths, the interaction occurs in extremely homogeneous initial conditions and allows the required resolution to distinguish between fluid and kinetic nonlinearities in the LW spectrum. At low $k\lambda_D$, LDI is observed via the existence of multiple LWs, both counterpropagating and copropagating. As $k\lambda_D$ increases, the amplitudes of the daughter waves from the LDI cascade drop below detection threshold, and a single frequency-broadened LW is observed, whose width is qualitatively consistent with a model for nonlinear frequency shifts due to electron trapping. The transition where strong LDI is no longer detected occurs near $k\lambda_D \sim 0.29$ and is qualitatively consistent with 1D collisionless simulations, as well as a 3D theory of the competition between LDI and the LW trapped particle frequency shift induced self-focusing (LWSF).

The experiments were performed using the TRIDENT laser facility [8], and the layout is given in Fig. 1. The plasma is generated with two 200 ± 15 J heater beams of 527 nm light in a 1.2 ns flat-top pulse directed onto a 13 μm thick CH (parylene-N) target. The laser beams are focused with $f/6$ lenses through a random phase plate producing a zero-to-zero spot size of $\sim$600 μm diameter. The electron densities produced are $n_e \sim 10^{20}$ cm^{-3} with electron temperatures in the range of $T_e = 500$–700 eV. A nearly diffraction-limited 527 nm interaction beam is directed parallel to the surface of the target creating a single hot spot (SHS) near the center of the plasma column [7]. The SHS laser is focused to a $\sim$2 μm spot using a $f/4.5$ lens and has a Strehl ratio of $\sim$0.5. The SHS interaction beam produces a peak intensity that can be varied from 10^{14}–10^{16} W/cm^2 with a pulse width of $\sim$200 ps. A 351 nm Thomson probe beam was used to measure driven waves associated with SRS ($k\lambda_D \sim 0.2$–0.4) copropagating with the SHS interaction beam with the geometry shown in Fig. 1. The Thomson probe was also used to characterize T_e by scattering from thermal-level ion acoustic waves. Driven waves from LDI, counterpropagating

 © 2005 The American Physical Society

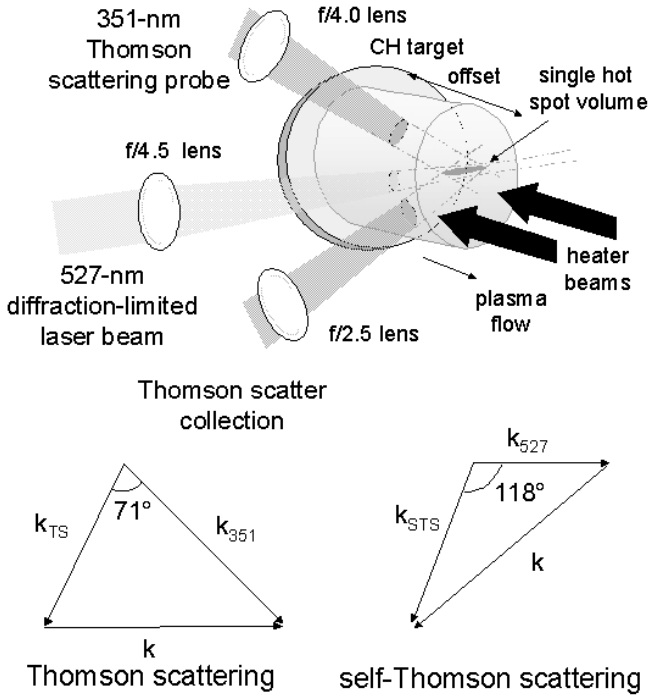

FIG. 1. Schematic diagram of the experimental setup.

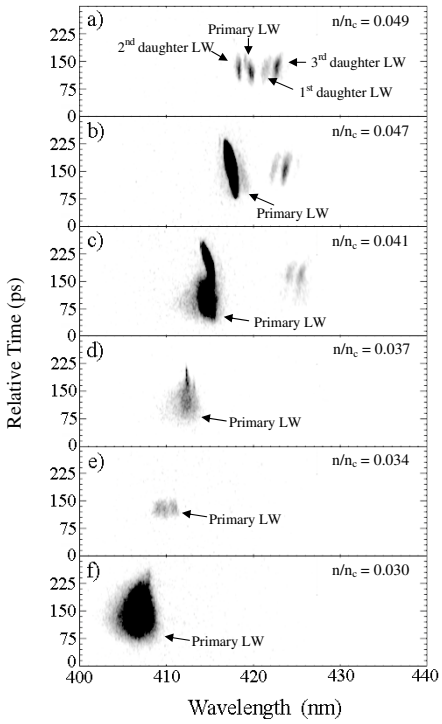

FIG. 2. Thomson streak records of Langmuir waves at six different average values of $k\lambda_D$. For the six shots the electron temperature was 620 eV at the center of each record and the average values for $k\lambda_D$ and the SHS intensity were (a) $k\lambda_D = 0.267$, $I_0 = 4.4 \times 10^{15}$ W/cm^2, (b) $k\lambda_D = 0.276$, $I_0 = 3.1 \times 10^{15}$ W/cm^2, (c) $k\lambda_D = 0.296$, $I_0 = 4.4 \times 10^{15}$ W/cm^2, (d) $k\lambda_D = 0.316$, $I_0 = 8.6 \times 10^{15}$ W/cm^2, (e) $k\lambda_D = 0.33$, $I_0 = 2.6 \times 10^{15}$ W/cm^2, and (f) $k\lambda_D = 0.352$, $I_0 = 1.1 \times 10^{16}$ W/cm^2.

with respect to the SHS beam, were measured using self-Thomson scattering (where the interaction beam serves as its own probe) with the geometry shown in Fig. 1. The electron density was changed by varying the distance between the target and the SHS, which is the primary method of systematically changing $k\lambda_D$ [9]. However, $k\lambda_D$ also decreases slightly ($k\Delta\lambda_D \sim 0.05$) on each target shot as the background plasma cools from ~700 to ~500 eV during the SHS interaction pulse.

Figure 2 shows the Thomson scattering streak records for six different values of $k\lambda_D$ ranging from 0.27 to 0.35 at the peak of the SHS pulse. At small $k\lambda_D$ [Fig. 2(a)] the LW spectra have multiple waves consistent with the LDI which has been observed in previous SHS experiments [10]. As $k\lambda_D$ increases, the daughter LDI LWs drop below detection levels, and the SRS primary LW spectra become broadened towards lower electrostatic wave frequencies (shorter scattered light wavelengths), consistent with the nonlinear frequency shift due to electron trapping. Over the range of $k\lambda_D$ scanned here there is clearly a transition in the LW spectra. This assertion is supported by a few key elements in these measurements. The width of each peak of the multiwave spectra is $\Delta\lambda \sim 1$–2 Å while the frequency-broadened spectrum of Fig. 2(f) is $\Delta\lambda \sim 60$ Å. The fact that the LW spectra in Figs. 2(a)–2(c) can be measured with such high resolution indicates that the SHS interaction volume is highly uniform, and inhomogenities cannot account for the frequency-broadened spectra. The strongest evidence that the frequency broadening is the result of a qualitative change in nonlinear behavior comes from the Thomson streak record in Fig. 2(c). As $k\lambda_D$ decreases in time, the broad LW spectrum narrows, and LDI turns on abruptly, likely due to the LDI threshold. The key consideration is to determine what mechanisms could be responsible for the different Langmuir wave spectra in the high and low $k\lambda_D$ regimes.

The multiwave spectra in Fig. 2(a) are attributed to LDI. The two waves on the left, the primary SRS and the 2nd LDI daughter LW copropagating, are measured directly with the 351 nm Thomson scattering beam. The two waves on the right, 1st and 3rd LDI daughter LWs counterpropagating with some finite $k_\perp$ with respect to the primary SRS LW, are measured via self-Thomson scattering from the 527 nm SHS beam. To support this, the measured scattered light wavelengths are compared with the values obtained from LDI theory. The change in wave number for each LDI daughter LW is $\Delta k\lambda_D \approx \frac{2}{3}\frac{c_s}{v_e}$, where c_s is the sound speed. The frequency of each LDI step, both copropagating and counterpropagating, can then be calculated from the Bohm-Gross dispersion relationship for Langmuir waves: $\omega_i \sim \omega_p(1 + \frac{3}{2}\Theta^2)$, where $\Theta = k\lambda_D - i\Delta k\lambda_D$, ω_p is the electron plasma frequency, and i is an integer representing the ith daughter Langmuir wave, with odd i counterpropagating and even i copropagating with respect to the pri-

mary Langmuir wave. Assuming the 351 nm light is scattered by the copropagating waves and the 527 nm light is scattered by the counterpropagating waves, the calculated scattered light wavelength for the SRS LW and the first three LDI LWs is $\lambda_0 \sim 421.1$ nm , $\lambda_1 \sim 422.8$ nm, $\lambda_2 \sim 419.8$ nm, and $\lambda_3 \sim 424.1$ nm, and the observations in Fig. 2(a) are $\lambda_0 \sim 421.1$ nm, $\lambda_1 \sim 422.8$ nm, $\lambda_2 \sim 419.7$ nm, and $\lambda_3 \sim 424.1$ nm.

A lower bound on the SRS LW amplitude is obtained by ignoring damping, diffraction, and refraction from Eq. (3) of Ref. [2] to obtain, for every scattered light pulse, in the scattered light frame, $d\sqrt{R}/dt < 0.25\omega_0(n_e/n_c)(\omega_b/\omega_p)^2$ where from Poisson's equation $(\omega_b/\omega_p)^2$ is the density fluctuation level, ω_b is the bounce frequency (the frequency at which a trapped particle makes a round trip in the potential well), n_e/n_c is the ratio of the plasma density to the critical density for the incident laser light, R is the ratio of the incident to the reflected laser power, and ω_0 is the incident laser frequency. For $n_e/n_c \ll 1$, $t < L/c = 7F^2\lambda/c$, so that $(\omega_b/\omega_p)^2 > (2/\pi)(n_c/n_e)\sqrt{R}/7F^2$, where L is the FWHM length of the laser hot spot, λ is the wavelength of the incident laser light, F is the lens focal length ratio, and c is the speed of light. In the LDI regime, R is observed to be at least 0.01, implying $\omega_b/\omega_p > 0.09$. The trapped-electron LW frequency shift is then $\sim 0.01\omega_p$, comparable to $2kc_s$, and hence LDI is in the strong trapping regime.

As the plasma density decreases, thus increasing $k\lambda_D$, LDI is no longer detected, and the SRS LW becomes frequency broadened [Figs. 2(c)–2(f)]. Experimentally, the details of the frequency shift may be obscured by the limits of the instruments. For our experimental temporal resolution, ~30 ps, one cannot discern between frequency broadening and time-dependent frequency shifts that might occur on much faster time scales (~100 fs). However, there are several characteristics of the spectra which indicate that the frequency broadening is due to trapping. The spectra are asymmetrically broadened towards lower electrostatic frequencies, consistent with a trapping-induced frequency shift. This is in contrast to the expected broadening due to dissipative mechanisms, such as Landau damping, which would produce symmetric broadening. In Fig. 2(c), where both LDI and broadened spectra are observed, the LW amplitude is similar in both regimes based on the magnitude of Thomson scattered light so that $\omega_b/\omega_p \sim 0.1$–$0.2$. Stronger trapping is expected at higher values of $k\lambda_D$ since there are more electrons at lower v_ϕ/v_e. The width of the spectral broadening in these experiments, $\delta\omega/\omega_p \sim 0.01$–$0.03$, is comparable to the nonlinear frequency shift due to trapping obtained from classical estimates [11] with $\omega_b/\omega_p \sim 0.09$. However, a direct comparison to this theory is unwarranted due to the dynamic behavior of the SRS process, nonadiabatic modifications to the electron distribution function due to trapping, and other higher dimensional effects. 1D reduced-particle-in-cell (RPIC) [12] simulations of SRS that include a transverse side loss model to account for the finite width of the SHS have led to a more detailed picture of trapping saturation that involves a complex spatiotemporal behavior of the scattered light and electrostatic waves [13]. In the scenario of Ref. [13], it is observed that trapping takes place in solitary intense pulses of LWs, growing in amplitude as they move toward the laser entrance. In these pulses the potential is much greater than the spatially

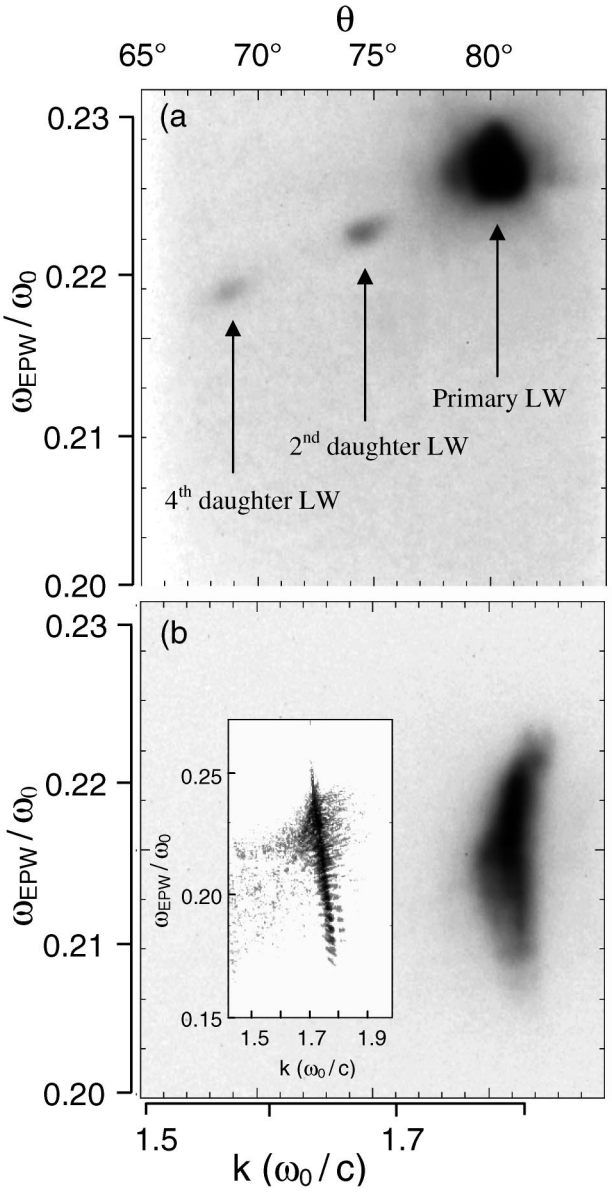

FIG. 3. Thomson scattering LW (ω, k) spectrum for (a) $k\lambda_D \sim 0.29$ showing the primary SRS LW and two copropagating LDI daughter LWs and for (b) $k\lambda_D \sim 0.34$ in the kinetic regime showing a broad frequency spectrum with a narrow wave-number spectrum. The inset in (b) shows a PIC simulation at $k\lambda_D = 0.30$ in which the (ω, k) spectrum is broad in ω and narrow in k, qualitatively consistent with the measurement. Electron trapping is observed in phase space for the simulation.

averaged potential, so trapping is indeed expected based on the above estimates. The continuous frequency spread is the result of chirping of the electrostatic wave frequency as the wave amplitude and therefore its frequency shift, due to trapping, undergos large excursions associated with the pulse behavior. A third key characteristic is the LW (ω, k) spectrum in the trapping regime, which we discuss next.

The Thomson scattered light was resolved in both wavelength and scattering angle and can be directly correlated to the (ω, k) spectra [14]. Figure 3(a) shows the (ω, k) spectrum in the LDI regime ($k\lambda_D \sim 0.29$), and the discrete LDI steps are clearly resolved and cover a relatively broad range of k space consistent with LDI theory and the Bohm-Gross dispersion relation. Measurements of LDI have been made previously, but the individual LDI steps have not been resolved [15–17]. Such spectra cannot be readily distinguished from strong Langmuir turbulence [18,19], or broadening due to electron trapping. As $k\lambda_D$ is increased to $\sim$0.34, the (ω, k) spectrum is frequency broadened with a relatively narrow k [Fig. 3(b)], $\Delta k \sim 0.032(\omega_0/c)$. In the case of LDI, the difference between the primary LW and the 4th daughter LDI step is $\Delta k \sim 0.250(\omega_0/c)$ over a similar range of frequencies as the broadened spectrum, a factor of 8 broader. This spectrum, broad in frequency and narrow in wave number, is qualitatively consistent with spatially and temporally averaged spectra calculated in Ref. [13] and shown in the inset of Fig. 3(b); i.e., both are broad in frequency and narrow in wave number. In these simulations, the spectrum is a result of the interplay of the time-dependent trapping frequency shift of the electrostatic wave and parametric ω and $\boldsymbol{k}$ matching and thus indicates that the measured spectrum is consistent with electron trapping. Similar observations have been made both in experiments and in simulations for $k\lambda_D \sim 0.38$, but for different plasma conditions using a 10.6 μm interaction laser [20].

The measurements of the LW spectra in these experiments show a change that is consistent with a transition from a fluid dominated to a purely kinetic nonlinear regime for LWs. Measurements of LDI below $k\lambda_D \sim 0.29$ show that fluid (wave-wave) nonlinearities are dominant although kinetic effects may also play an important coexisting role in the nonlinear LW behavior. For $k\lambda_D \gtrsim 0.29$, LDI is no longer detected and the LW spectra become frequency broadened. In this regime, the LW amplitude estimates, the asymmetric spectral broadening of the order of trapped particle frequency shift estimates, and the very narrow wave-number spectra are evidence that nonlinear kinetic effects due to electron trapping are important for SRS LWs for large values of $k\lambda_D$. These results are qualitatively consistent with results of RPIC that show a transition from fluid to kinetic SRS LW nonlinearities and predict spectra similar to those observed [13]. The experimental data presented in this Letter suggest that the transition occurs near $k\lambda_D \sim 0.29$, possibly somewhat higher than predicted by the RPIC model [5,6] which might be attributed to the higher dimensionality of the experiments including effects such as transverse supersonic flows [21] and LWSF [22].

Future experiments will use a gas jet target with low Z gas to create the preformed plasma for the SHS experiments. This should minimize thermal effects and eliminate supersonic transverse plasma flows, in which case, it may be possible to compare quantitatively simulations with experimental results.

We wish to acknowledge useful discussions with J. Fernández, D. Barnes, E. S. Dodd, and J. Kindel. These experiments would not have been possible without the technical expertise of R. Gibson, F. Archuleta, R. Gonzales, T. Hurry, N. Okamoto, and T. Ortiz of the TRIDENT laser crew, and R. Perea of Target Fabrication. This work was performed under the auspices of the DOE/NNSA by LANL under Contract No. W-7405-ENG-36.

[1] J. D. Lindl, *Inertial Confinement Fusion. The Quest for Ignition and Energy Gain Using Indirect Drive* (Springer, New York, 1998).
[2] B. J. MacGowan *et al.*, Phys. Plasmas **3**, 2029 (1996).
[3] D. A. Russell, D. F. DuBois, and H. A. Rose, Phys. Plasmas **6**, 1294 (1999).
[4] H. A. Rose and D. A. Russell, Phys. Plasmas **8**, 4784 (2001).
[5] H. X. Vu, D. F. DuBois, and B. Bezzerides, Phys. Rev. Lett. **86**, 4306 (2001).
[6] H. X. Vu, D. F. DuBois, and B. Bezzerides, Phys. Plasmas **9**, 1745 (2002).
[7] D. S. Montgomery *et al.*, Laser Part. Beams **17**, 349 (1999).
[8] N. K. Moncur *et al.*, Appl. Opt. **34**, 4274 (1995).
[9] Density is determined from the measured backscattered light using the linear dispersion relationship and measured background electron temperatures. Local heating in the hot spot has not been considered in this Letter, which would increase the quoted values of $k\lambda_D$.
[10] D. S. Montgomery *et al.*, Phys. Plasmas **9**, 2311 (2002).
[11] G. J. Morales and T. M. O'Neil, Phys. Rev. Lett. **28**, 417 (1972); W. M. Manheimer and R. W. Flynn, Phys. Fluids **14**, 2393 (1971); R. L. Dewar, Phys. Fluids **15**, 712 (1972).
[12] H. X. Vu, B. Bezzerides, and D. F. DuBois, J. Comput. Phys. **156**, 12 (1999).
[13] H. X. Vu *et al.* (to be published).
[14] H. A. Baldis and C. J. Walsh, Appl. Phys. B **28**, 293 (1982).
[15] K. L. Baker *et al.*, Phys. Rev. Lett. **77**, 67 (1996).
[16] S. Depierreux *et al.*, Phys. Rev. Lett. **84**, 2869 (2000).
[17] S. Depierreux *et al.*, Phys. Rev. Lett. **89**, 045001 (2002).
[18] D. S. Montgomery, Phys. Rev. Lett. **86**, 3686 (2001).
[19] D. Pesme *et al.*, Phys. Rev. Lett. **86**, 3687 (2001).
[20] M. J. Everett *et al.*, Phys. Rev. Lett. **74**, 1355 (1995).
[21] D. S. Montgomery *et al.*, Phys. Rev. Lett. **84**, 678 (2000).
[22] H. A. Rose, Phys. Plasmas **12**, 012318 (2005).